J. Biochem. 2021;170(1):79–87 doi:10.1093/jb/mvab022

JB THE JOURNAL OF BIOCHEMISTRY

Kinetic analysis of the inhibition mechanism of bovine mitochondrial F_1-ATPase inhibitory protein using biochemical assay

Received November 25, 2020; accepted February 24, 2021; published online March 9, 2021

Ryohei Kobayashi , Sougo Mori, Hiroshi Ueno and Hiroyuki Noji*

Department of Applied Chemistry, Graduate School of Engineering, The University of Tokyo, 7-3-1 Hongo, Bunkyo-ku, Tokyo 113-8656, Japan

*Hiroyuki Noji, Department of Applied Chemistry, Graduate School of Engineering, The University of Tokyo, Tokyo 113-8656, Japan. Tel: +81-3-5841-7252, Fax: +81-3-5841-1872, email: hnoji@g.ecc.u-tokyo.ac.jp

Graphical Abstract

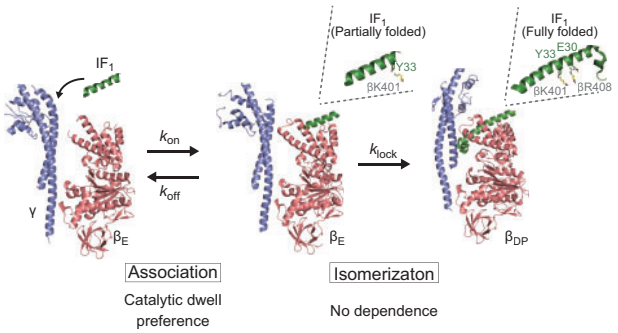

ATPase inhibitory factor 1 (IF_1) is a mitochondrial regulatory protein that blocks ATP hydrolysis of F_1-ATPase, by inserting its *N*-terminus into the rotor–stator interface of F_1-ATPase. Although previous studies have proposed a two-step model for IF_1-mediated inhibition, the underlying molecular mechanism remains unclear. Here, we analysed the kinetics of IF_1-mediated inhibition under a wide range of [ATP]s and [IF_1]s, using bovine mitochondrial IF_1 and F_1-ATPase. Typical hyperbolic curves of inhibition rates with [IF_1]s were observed at all [ATP]s tested, suggesting a two-step mechanism: the initial association of IF_1 to F_1-ATPase and the locking process, where IF_1 blocks rotation by inserting its *N*-terminus. The initial association was dependent on ATP. Considering two principal rotation dwells, binding dwell and catalytic dwell, in F_1-ATPase, this result means that IF_1 associates with F_1-ATPase in the catalytic-waiting state. In contrast, the isomerization process to the locking state was almost independent of ATP, suggesting that it is also independent of the F_1-ATPase state. Further, we investigated the role of Glu30 or Tyr33 of IF_1 in the two-step mechanism. Kinetic analysis showed that Glu30 is involved in the isomerization, whereas Tyr33 contributes to the initial association. Based on these findings, we propose an IF_1-mediated inhibition scheme.

Keywords: ATPase inhibitory factor 1 (IF_1); ATP synthase; enzyme kinetics; F_1-ATPase; rotary molecular motor.

Abbreviations: *b*MF_1, F_1 from bovine mitochondria; F_1, F_1-ATPase; F_oF_1, F_oF_1-ATP synthase; GFP, green fluorescent protein; His-tag; histidine tag; HEPES, 2-[4-(2-hydroxyethyl)piperazin-1-yl]ethanesulfonic acid; IF_1, ATPase Inhibitory factor 1; KPi; potassium phosphate buffer; MALDI-TOF/TOF, Matrix Assisted Laser Desorption/Ionization—Time-of-Flight/Time-of-Flight mass spectrometer; *pmf*, proton motive force; SDS-PAGE, sodium dodecyl sulfate polyacrylamide gel electrophoresis; TEV, tobacco etch virus; TF_1, F_1 from thermophilic *Bacillus* PS3.

ATP synthase, also termed as F_oF_1-ATP synthase (F_oF_1), is ubiquitously found in bacterial plasma membranes, chloroplast thylakoid membranes and mitochondrial inner membranes (*1*–*5*). It catalyzes ATP synthesis from ADP and inorganic phosphate (P_i) using proton motive force (*pmf*) across membranes. F_oF_1-ATP synthase consists of two reversible rotary motors, F_o and F_1. F_o, the membrane-embedded portion of ATP synthase, conducts proton translocation across the membrane, whereas F_1, the water-soluble portion, contains the catalytic centre domain for ATP synthesis. In the F_oF_1 complex, F_o and F_1 are connected by the common rotary shaft and the peripheral stalk, enabling the interconversion of *pmf* and the chemical potential of ATP. Under physiological conditions with sufficiently high *pmf* level, F_o reverses the rotation of F_1, inducing ATP synthesis. When *pmf* is low or diminished, F_1 hydrolyzes ATP to rotate F_o in the opposite direction, resulting in active proton pumping to form *pmf*.

F_1 hydrolyzes ATP to ADP and P_i when isolated from F_o (*6*, *7*). $\alpha_3\beta_3\gamma$ is the minimum component of a rotary molecular motor. Three α subunits and three β subunits are arranged alternately to form the $\alpha_3\beta_3$ stator ring, of which the central rotary shaft, the γ subunit, is inserted into the central cavity (*8*, *9*). The catalytic reaction centres are located on the αβ interface, mainly on the β subunit. During ATP hydrolysis, the γ subunit of F_1 rotates against the $\alpha_3\beta_3$-ring in anticlockwise direction when viewed from the F_o side (*5*). Crystal structures of bovine mitochondrial F_1-

ATPase (bMF$_1$) showed asymmetric features of nucleotide occupancy and the conformational states of the three β subunits (*8*, *10–12*). One β subunit, designated β_{TP}, preferentially binds to an ATP analogue, AMP-PNP, whereas another one, β_{DP}, binds to ADP and P_i or P_i analogues, representing the catalytically active state. The third one, β_E, has no nucleotides, although some crystal structures show that it has phosphate (*9*), thiophosphate (*11*) or sulfate ions (*12*), suggesting that β_E represents the phosphate releasing state (*13*). Both β_{TP} and β_{DP} adopt a closed conformational state in which the *C*-terminal domain swings toward the γ subunit, wrapping the bound nucleotide, whereas β_E assumes an open conformation.

The coupling reaction scheme for the rotation and catalysis of bMF$_1$ was recently studied in a single-molecule rotation study (*14*). Similar to the reaction scheme for thermophilic F$_1$ (TF$_1$), bMF$_1$ makes rotation with 120° steps, each resolved into 80° and 40° substeps. The 80° and 40° substeps are triggered by ATP binding and hydrolysis, respectively. Therefore, the dwelling states before the 80° and 40° substeps are referred to as 'binding dwell' and 'catalytic dwell', respectively. In addition, bMF$_1$ exhibits a short transient pause between the binding dwell and the catalytic dwell. The reaction step involved in the short transient pause remains to be identified. Previous studies have shown that the crystal structures of bMF$_1$ in the ground state or relevant states correspond to the catalytic dwell in the rotation assay (*14–16*).

There are diverse mechanisms for the suppression of ATP hydrolysis by F$_1$, which is generally detrimental to cells (*17–19*). The self-inhibition of F$_1$, termed ADP inhibition, is the most universal mechanism for F$_1$ inhibition (*14*, *20*, *21*). Inhibitory factor 1 (IF$_1$) of mitochondrial F$_1$ inhibits unfavourable ATPase. Under inhibitory conditions, IF$_1$ associates with F$_1$ to block ATP hydrolysis by inserting its *N*-terminal region into F$_o$F$_1$-ATP synthase, which results in mechanical blockage of rotation and catalysis. Bovine mitochondrial IF$_1$ is composed of 84 amino acid residues. IF$_1$ inhibits the function of F$_o$F$_1$-ATP synthase under hydrolytic condition to prevent wasteful consumption of ATP. Thus, it is an unidirectional inhibitor of F$_o$F$_1$-ATP synthase (*22*, *23*), although several reports have suggested that IF$_1$ also has an inhibitory effect under synthesized condition (*24*, *25*). Among the 84 residues in bovine IF$_1$, the *N*-terminus is responsible for the inhibition of F$_o$F$_1$-ATP synthase, forming a long α-helix when bound to F$_1$. When isolated from F$_1$, the *N*-terminus of IF$_1$ is intrinsically disordered (*26*). Native IF$_1$ forms a homodimer associating at the *C*-terminal region (*27*, *28*). Deletion of *C*-terminus residues 61–84 produces a stable monomeric form of IF$_1$ without the loss of inhibition activity (*28*, *29*). Thus, the *C*-terminus deleted form of IF$_1$ (termed IF_1^{1-60} hereafter) provides a simple platform for biochemical and structural analyses of IF$_1$ (*28*, *30*, *31*). Biochemical assay showed that the fusion of green fluorescent protein (GFP) and 6 histidine tag (His-tag) to the *C*-terminus in IF_1^{1-60} (IF_1^{1-60}GFPHis) has little impact on its inhibitory capacity (*30*).

The first crystal structure of the complex of bMF$_1$ and IF_1^{1-60} showed that the *N*-terminal helix of IF_1^{1-60} was deeply buried in the α_{DP}/β_{DP} interface in its locked state (*28*). Following this, the crystal structure of the bMF$_1$-$(IF_1^{1-60})_3$ complex was resolved, revealing that each of the three α/β interfaces was occupied with IF$_1$ (*31*). Each IF$_1$ bound to the α/β interface differed in conformation: IF$_1$ at the α_{DP}/β_{DP} interface showed the most folded state, as found in the first bMF$_1$-IF$_1$ structure; IF$_1$ at α_{TP}/β_{TP} showed partially folded α-helix with unfolded *N*-terminal region; and IF$_1$ at α_E/β_E was largely disordered. These findings suggest progressive conformational isomerization of IF$_1$ from a disordered state to the α-helical state, accompanying the conformational transition of the α/β pair from α_E/β_E to α_{DP}/β_{DP}. As the conformational transition of the α/β pair is tightly coupled with γ rotation, the progressive conformational isomerization model inevitably assumes that IF inhibition accompanies γ rotation (Fig. 1A). Comprehensive studies of mutagenesis based on the crystal structure revealed that Glu30 and Tyr33 of IF$_1$ are particularly critical for IF$_1$ inhibition. Glu30 and Tyr33 form a salt bridge and hydrophobic interaction with a residue of the β subunit, respectively. Ala substitution causes a loss of the inhibitory activity of IF$_1$ (*30*). However, the roles of these residues in the proposed progressive conformational change model remain to be elucidated.

Biochemical studies have revealed that IF$_1$ inhibition requires catalytic turnover of F$_1$; in the absence of ATP, IF$_1$ only shows slow and partial inhibition of F$_1$ (*32*, *33*). In the presence of ATP, IF$_1$ shows rapid inhibition during turnover (*34*). Kinetic analyses showed that the rate constant of IF$_1$-mediated inhibition increases with [ATP], although some complex behaviours of IF$_1$ inhibition were observed, such as a decrease in the inhibition rate at the mM range of

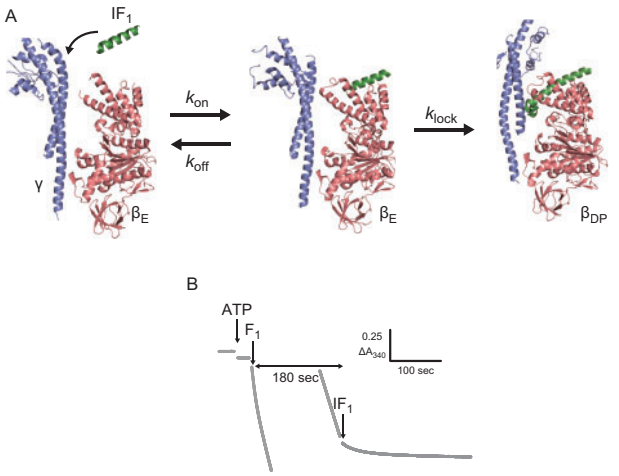

Fig. 1. Experimental concept and procedure. (**A**) Schematic image of inhibition by IF$_1$. IF$_1$ loosely associates with the α_E and β_E subunits. Then, IF$_1$ is deeply inserted into the $\alpha_{DP}\beta_{DP}$ interface (PDB: 2JDI and 4TT3). The initial association and the following isomerization are represented by three rate constants, k_{on}, k_{off} and k_{lock}. (**B**) Time course of 340 nm NADH absorbance at 1 mM ATP and 1 μM IF_1^{1-60}. At 180 s after F$_1$ addition, IF_1^{1-60} was added to the reaction mixture and ATPase activity decreased. To see this figure in colour, go online.

[ATP] (*32*, *33*, *35*). The correlation of IF_1 inhibition with occupancy of the catalytic site was also studied (*32*, *33*, *36*). Based on kinetic analyses, an ATP-dependent two-step model has been proposed for IF_1-mediated inhibition (*35*, *37*, *38*). The two-step model suggests that the rate constant of IF_1-mediated inhibition should increase with [IF_1], reaching an ATP-dependent plateau. However, comprehensive kinetic analysis covering a wide range of IF_1 and ATP concentrations to confirm the expected hyperbolic curves has not been performed yet.

In this study, we studied the kinetics of bMF_1 inhibition by bovine mitochondrial IF_1 with an NADH-coupled ATP-regenerating system, using a wide range of [ATP] from 100 nM to 1 mM with [IF_1] from 0.05 to 40 μM. The resultant rate constant of IF_1-mediated inhibition showed typical hyperbolic curves for [IF_1] at each [ATP], consistent with the two-step model. We then investigated the IF_1 mutants IF_1(E30A) and IF_1(Y33A) to study the effects of Glu30 and Tyr33, respectively, on the kinetics of IF_1 inhibition. Based on the results as well as the established reaction scheme for catalysis and rotation of bMF_1 (*14*), we propose an IF_1 inhibition scheme.

Materials and Methods

Construct and purification of IF_1

An expression plasmid encoding residues 1–60 of bovine IF_1 was constructed as follows: His-tag and TEV site were fused to the *N*-terminal region, and the linker and mScarlet sequences were fused to the *C*-terminal region. The resulting artificially synthesized construct was introduced into the pRSET-B plasmid, which encoded the protein IF_1^{1-60}mScarlet (hereafter referred to as wild-type IF_1^{1-60} or IF_1^{1-60}).

$IF_1^{1-60(\Delta mS)}$ was generated by deleting the linker and mScarlet sequences from the wild-type IF_1^{1-60} plasmid. The single-point amino acid mutants, E30A and Y33A, were introduced into the wild-type IF_1^{1-60} plasmid. The sequence encoding IF_1^{1-60} or a mutation was amplified by PCR. After gel electrophoresis and purification, the product was digested with two restriction enzymes and cloned into the vector wild-type IF_1^{1-60} plasmid, digested with the same restriction enzymes. The sequences of the recombinant plasmids for IF_1 were confirmed by Fasmac sequencing service (Fasmac, Japan).

Cells of *Escherichia coli* C43 were transformed with the constructed plasmids and grown in LB medium containing 100 μg/mL carbenicillin at 37°C for 4 h as a preculture. The culture medium was then transferred to SB medium containing 100 μg/mL carbenicillin at 37°C. When the absorbance of the culture was 0.6 at 600 nm (for ~4 h), isopropyl-β-D-thiogalactopyranoside (IPTG) was added at a final concentration of 1 mM to induce protein expression. After 24 h of growth at 20°C, cells were harvested by centrifugation (7000×*g*, 8 min, 4°C). Subsequent procedures were performed at 4°C, except for the gel-filtration process. The harvested cells were suspended in buffer A [50 mM KP_i (pH 7.5), 200 mM KCl, 10% Glycerol and 25 mM Imidazole], disrupted by an ultrasound disintegrator and subjected to ultracentrifugation (81,000×*g*, 20 min). The supernatant was applied to Ni-Sepharose FF resin (GE Healthcare) equilibrated in buffer A. After binding IF_1 to the resin, it was washed with 10 volumes of buffer A. IF_1 was eluted with elution buffer [50 mM KP_i (pH 7.5), 200 mM KCl, 10% glycerol and 500 mM imidazole].

To remove His-tag, TEV protease was used. The eluted fractions containing the proteins were concentrated with a centrifugal concentrator (3 kDa for $IF_1^{1-60(\Delta mS)}$ and 10 kDa for wild-type IF_1^{1-60} and mutants; Centricon50; Millipore Corp.). The concentrated fractions were diluted 20-fold with TEV treatment buffer [20 mM KP_i (pH 8.0), 50 mM NaCl 0.04% 2-mercaptoethanol, and 0.1 mg/mL TEV protease]. After treatment for 16 h at 4°C, the solution was concentrated with a centrifugal concentrator and diluted 30-fold with buffer A. The resultant solution was applied to a Ni-Sepharose FF resin. The flow-through and wash fractions were concentrated with a centrifugal concentrator after adding DTT at a final concentration of 5 mM. The resulting samples were further purified by passing through a gel-filtration column (Superdex 75 for $IF_1^{1-60(\Delta mS)}$, and Superdex 200 for wild-type IF_1^{1-60} and mutants; GE Healthcare) equilibrated with Gel-filtration buffer [20 mM HEPES-KOH (pH7.5), 100 mM KCl and 10% glycerol]. If necessary, the fractions were concentrated with a centrifugal concentrator. The concentration of IF_1 was determined based on the absorbance at 280 nm. The purified samples were flash-frozen in liquid nitrogen and stored at −80°C before use. Their molecular masses were verified by SDS-PAGE (sodium dodecyl sulfate polyacrylamide gel electrophoresis) analysis (Supplementary Fig. S1). Further confirmation of the molecular masses for wild-type IF_1^{1-60} and $IF_1^{1-60(\Delta mS)}$ was performed by MALDI-TOF/TOF mass spectrometry (Genomine. Inc., Korea) (Supplementary Table S1).

Construct and purification of bMF_1

bMF_1 was prepared as previously described (*14*) with slight modifications. We removed ATP from buffers A, B and gel-filtration buffer for measurements of ATPase activity at low ATP conditions because the carryover ATP from the purified bMF_1 sample to the cuvette was not negligible under these conditions. The ATPase activity of bMF_1 purified without ATP was identical to that purified with ATP.

Biochemical assay with NADH-coupled ATP-regenerating system

As previously reported (*14*), the ATPase activity of bMF_1 was measured using a spectrometer at 25°C in HEPES-KOH (pH 7.5) containing KCl, $MgCl_2$ and an ATP-regenerating system supplemented with NADH and lactate dehydrogenase. The ATPase reaction was initiated by adding purified bMF_1.

IF_1 was added 180 s after the addition of bMF_1 to avoid ADP inhibition. The change in NADH absorbance was monitored for over 10 min. All data points were measured at least in triplicate. The apparent rate constants for IF_1 inhibition ($k_{inhibition}^{app}$) were measured from the exponential decay of ATPase activity after IF_1 addition, using the following equation:

$$y(t) - y_0 = V_\infty t + \frac{V_0 - V_\infty}{k_{inhibition}^{app}}\left\{1 - \exp\left(-k_{inhibition}^{app} t\right)\right\} \quad (1)$$

where $y(t)$ and y_0 are the absorbances at time points t and 0 after IF_1 addition, respectively, and V_0 and V_∞ are the initial and final rates of reaction, respectively. For precise fitting, we have fitted the time course 60 s after IF_1 injection to remove noise caused by solution injection. Examples of V_0 and V_∞, estimated in Fig. 2B at 1 mM ATP, were shown in Supplementary Fig. S6.

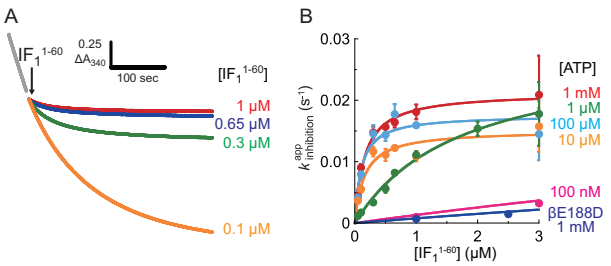

Fig. 2. Kinetic analysis of IF_1 inhibition in bMF_1. (**A**) Time course of IF_1 inhibition at 1 mM ATP. Colour represents different IF_1^{1-60} concentrations; (Red) 1 μM, (Blue) 0.65 μM, (Green) 0.3 μM, and (Orange) 0.1 μM. The final concentration of bMF_1 was 10 nM. (**B**) Determined $k_{inhibition}^{app}$ plotted against [IF_1^{1-60}]s. The mean value and SD for each data point in (B) are shown with circles and error bars, respectively ($n = 3$ for each measurement). Solid line represents the fitting curve of Eq. 2. For wider [IF_1^{1-60}] range of wild-type bMF_1 at 100 nM ATP and bMF_1(βE188D) at 1 mM ATP, see Supplementary Fig. S4. To see this figure in colour, go online.

Modelling the two-step reaction of IF$_1$ inhibition

The kinetic scheme is as follows:

$$F_1 + IF_1 \underset{k_{off}}{\overset{k_{on}}{\rightleftarrows}} F_1 \cdot IF_1 \overset{k_{lock}}{\rightarrow} F_1 \cdot IF_1^{lock} \qquad \text{(Scheme 1)}$$

where k_{on} is the rate constant for IF_1 binding to F_1, k_{off} is the rate constant for IF_1 release from F_1, and k_{lock} is the rate constant for isomerization to the locked state. F_1 and $F_1 \cdot IF_1$ are active and $F_1 \cdot IF_1^{lock}$ is inactive. In the first step, IF_1 loosely binds to F_1, forming an intermediate state. Following this, IF_1 is irreversibly locked, forming a dead-end complex. For derivation of $k_{inhibition}^{app}$, see the Supplemental text.

Results

Preparation of *IF$_1$* protein

C-terminal residues of IF_1^{1-60} in bovine IF_1 were fused with mScarlet, a bright monomeric red fluorescent protein with a short linker sequence, to enhance its expression in *E. coli*, as previously described (*30*). The fusion IF_1 is hereafter referred to as wild-type IF_1^{1-60} or IF_1^{1-60} for simplicity, unless mentioned otherwise. For comparison, we also purified $IF_1^{1-60(\Delta mS)}$ lacking the linker sequence and the mScarlet domain. For the preparation of IF_1^{1-60}(E30A) or IF_1^{1-60}(Y33A), a single point mutation was introduced into the wild-type IF_1^{1-60} plasmid. For purification with an Ni-Sepharose column, the His-tag and TEV recognition sequences were fused to the *N*-terminal region of the IF_1 proteins. After collecting the eluted fractions from the Ni-Sepharose column, the His-tag was cleaved with TEV-protease. The resultant products were identified by SDS-PAGE analysis (Supplementary Fig. S1) and mass spectroscopy (Supplementary Table S1).

Time course of *IF$_1$*-mediated inhibition

ATP hydrolysis activity of bMF_1 was monitored using an ATP regenerating system. The decay of NADH absorbance at 340 nm represents ATP hydrolysis leading to NADH oxidation. Upon injection, bMF_1 initially showed rapid catalysis, followed by slow deceleration to reach steady-state catalysis (Fig. 1B). The slow auto-inactivation is a typical feature of ADP inhibition. Under the present conditions, bMF_1 activity almost reached steady state within 180 s (Supplementary Fig. S2). Subsequently, IF_1 was injected at 180 s after F_1 injection. Since the time constant for ADP inhibition at 1 μM ATP was longer than 400 s, ADP inhibition did not reach an equilibrium state at the time of IF_1 injection. However, additional analysis of IF_1 inhibition including ADP inhibition (Supplementary text and Supplementary Fig. S3) revealed that it has little impact on IF_1 kinetics, probably due to the slow and modest suppression at 1 μM ATP.

Fig. 2A shows the typical time courses of IF_1-mediated inhibition at 1 mM [ATP]. Immediately after the injection of IF_1^{1-60}, ATPase activity decreased, reaching almost zero activity. The time course of IF_1-mediated inhibition was well fitted with an exponential function (Eq. 1), giving the apparent rate constant of the inhibition, $k_{inhibition}^{app}$. The inhibition rate increased with [IF_1^{1-60}], reaching a plateau when [IF_1^{1-60}] was over 0.65 μM. We also measured the time courses of IF_1-mediated inhibition to determine $k_{inhibition}^{app}$ at all [ATP]s ranging from 100 nM to 1 mM. In Fig. 2B and Supplementary Fig. S4, data points of $k_{inhibition}^{app}$ are plotted against [IF_1^{1-60}] at all [ATP]s. At a given [ATP], $k_{inhibition}^{app}$ always increases with [IF_1^{1-60}] and reaches a plateau, following a hyperbolic curve. Further, we tested the inhibitory capacity of a monomer IF_1 without mScarlet ($IF_1^{1-60(\Delta mS)}$) and found that the result was almost identical to that of wild-type IF_1^{1-60} (Supplementary Fig. S5), suggesting that mScarlet in the *C*-terminal region did not affect the kinetics of IF_1-mediated inhibition. It should be noted that previous biochemical assay based on mutagenesis (*30*) showed monotonous enhancement of $k_{inhibition}^{app}$, whereas clear hyperbolic curve was observed in our assay. Such an apparent difference is attributable to low [IF_1] employed in the assay (*30*), which enabled to visualize the limited region of the hyperbolic curve in the two-step inhibition mechanism. Another possible reason for this discrepancy is the difference in experimental conditions: including pH, temperature and chemicals.

The observed hyperbolic curves suggest a two-step model, where IF_1 reversibly associates with F_1, and the resulting $F_1 \cdot IF_1$ complex isomerizes to the final locked state. Thus, we assume the following reaction scheme for IF_1-mediated inhibition:

$$F_1 + IF_1 \underset{k_{off}}{\overset{k_{on}}{\rightleftarrows}} F_1 \cdot IF_1 \overset{k_{lock}}{\rightarrow} F_1 \cdot IF_1^{lock} \qquad \text{(Scheme 1)}$$

where, $F_1 \cdot IF_1^{lock}$ represents the catalytically locked state of the $F_1 \cdot IF_1$ complex. k_{on} and k_{off} represent the rate constants of association and dissociation, respectively. k_{lock} is the rate constant of isomerization to the locked state. This scheme calculates the apparent rate constant of IF_1 inhibition, $k_{inhibition}^{app}$, as follows:

$$k_{inhibition}^{app} = \frac{[IF_1]}{K_M^{IF_1} + [IF_1]} \cdot k_{lock} \qquad (2)$$

$$K_M^{IF_1} \equiv \frac{k_{off} + k_{lock}}{k_{on}} \qquad (3)$$

The experimentally obtained data points at each [ATP] were well fitted with Eq. 2, giving k_{lock} and $K_M^{IF_1}$.

[ATP] dependence of k_{lock} and $K_M^{IF_1}$

Fig. 3A shows the plot of k_{lock} against [ATP]s. Although not well constant, k_{lock} was around 0.02 s^{-1} irrespective of [ATP]; this value is almost consistent with that estimated from previous studies (*39*, *40*). k_{lock} is evidently lower than the catalytic turnover rate, 1–200 s^{-1}, indicating that IF_1 transforms into the inhibitory locking state during the rotation of the γ subunit. Fig. 3B shows the plot of $K_M^{IF_1}$ against [ATP]. $K_M^{IF_1}$ was determined to be in the sub-μM to μM range, consistent with that of previous biochemical studies with isolated F_1 and sub-mitochondrial particles (*32–35*, *39*). $K_M^{IF_1}$ reveals a clear [ATP] dependence, decreasing from 27 to 0.1 μM when [ATP] is over 10 μM. Considering constant k_{lock} over [ATP], this means that the rate constant of IF_1 association to F_1 follows a hyperbolic increment with [ATP].

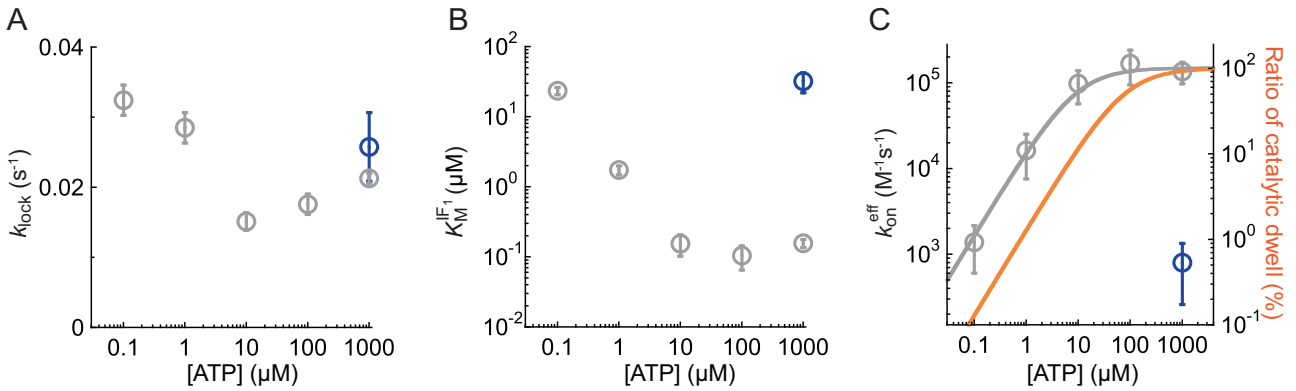

Fig 3. Fitted parameters derived from Fig. 2B and Supplementary Fig. S4. (**A**) k_{lock} and (**B**) $K_M^{IF_1}$. In (A) and (B), the circles and error bars in each data point represent the fitted parameter and fitting error determined in Fig. 2B and Supplementary Fig. S4. (**C**) The effective binding constant $k_{on}^{eff} \equiv k_{lock}/K_M^{IF_1}$. The gray line represents the fitting curve of Eq. 5 and the orange line represents the duty ratio of catalytic dwell against overall reaction time. The circles and error bars in each data point represent the mean value and the SD calculated from Fig. 3A and B. In Fig. 3A–C, grey and blue points represent the results for bMF$_1$(wild-type) at 0.1–1000 μM and bMF$_1$(βE188D) at 1 mM ATP, respectively. To see this figure in colour, go online.

Here, we define the effective rate constant of IF_1 association to F_1 as follows:

$$k_{on}^{eff} \equiv \frac{k_{lock}}{K_M^{IF_1}} \quad (4)$$

Fig. 3C shows the plot of k_{on}^{eff} against [ATP]. As expected, k_{on}^{eff} shows a typical hyperbolic saturation curve. Considering that IF_1 cannot bind ATP by itself, it is reasonable to attribute the ATP binding to F_1, *c.f.* IF_1 is predominantly associated with F_1 in the post-ATP-bound state. In light of the reaction scheme for rotation and catalysis, this means that IF_1 is not associated with F_1 in the binding dwell, but it preferentially associates with F_1 in the catalytic dwell.

With the assumption that IF_1 preferentially binds to F_1 in the catalytic dwell, we tested the mutant bMF$_1$(βE188D). Previous studies have shown that Glu188 of bMF$_1$ or the corresponding glutamic residues of other F_1s are the most critical residues for catalysis (*8*, *16*, *41*). Mutagenic substitution of Glu188 with aspartic acid largely retarded bMF$_1$ catalysis, lengthening the catalytic dwell by 400 times (*14*). We investigated IF_1-mediated inhibition of bMF$_1$(βE188D) at 1 mM [ATP] (Supplementary Fig. S7). Contrary to the expectation, bMF$_1$(βE188D) did not exhibit enhanced IF_1 inhibition rate compared with wild-type bMF$_1$ at saturating [ATP]s. The hyperbolic inhibition curve of bMF$_1$(βE188D) at 1 mM [ATP] was similar to that of wild-type bMF$_1$ at 100 nM [ATP], where the binding dwell is dominant (Fig. 2B and Supplementary Fig. S4). Considering that F_1 mediates two reactions through the catalytic dwell, hydrolysis and presumably inorganic phosphate release, the catalytic state and the conformation of bMF$_1$(βE188D) at the catalytic dwell maybe different from that of the wild-type in some aspects.

Mutation of Glu30 and Tyr33

A previous comprehensive mutagenetic study identified E30 and Y33 as the most critical residues for the inhibitory function of IF_1 (*31*). Although the mutants created by substituting these residues with alanine suppressed the activity down to an undetectable level (*30*), we reinvestigated these mutants, IF_1^{1-60}(E30A) and IF_1^{1-60}(Y33A), in our experimental setup.

Experiments were conducted using 1 mM [ATP]. Fig. 4A shows the time course of its inhibition by IF_1^{1-60}(E30A) at 0.5, 1 and 3 μM concentrations, which are similar to the range for wild-type IF_1^{1-60}. ATPase activity showed slight decay and reached steady state with some activity remaining. Compared to wild type, where the complete inhibition was observed (Fig. 2A), the inhibition by IF_1^{1-60}(E30A) was not irreversible. Based on the exponential fitting of the time courses in Eq. 1, $k_{inhibition}^{app}$ of IF_1^{1-60}(E30A) was determined (Fig. 4B, green) and found to be quite similar to that of wild-type IF_1^{1-60} (Fig. 4B, grey) at each [IF_1^{1-60}(E30A)]. The resultant k_{lock} and k_{on}^{eff} were almost consistent with those for the wild-type IF_1^{1-60} (Supplementary Table S2). These results show that the E30A mutant also follows a two-step mechanism for inhibition. However, IF_1^{1-60}(E30A)-mediated inhibition is evidently less efficient, as seen in the partial inhibition of ATPase activity. Fig. 4C shows the final ATPase activity observed at the end of the measurement (360 s after IF_1 injection). While wild-type IF_1 suppresses ATPase activity down to almost zero at each [IF_1^{1-60}], IF_1^{1-60}(E30A) suppresses ATPase activity down to only 20–40% at [IF_1^{1-60}(E30A)]s lower than 1 μM. Even at 3 μM [IF_1^{1-60}(E30A)], where $k_{inhibition}^{app}$ reached a plateau, a fraction of bMF$_1$ retained its activity.

The Y33A mutant, IF_1^{1-60}(Y33A), was also examined at 1 mM ATP. Fig. 4D shows the time course of its inhibition. This mutant required a significantly higher concentration of [IF_1^{1-60}(Y33A)], at least 10 μM [IF_1^{1-60}(Y33A)], to induce clear inhibition. However, in contrast to the E30A mutant, the Y33A mutant suppressed ATPase activity to almost zero (Fig. 4F). These observations suggest that the Y33A mutant has high inhibitory activity, although the time scale for its association with F_1 was significantly longer than that for the wild-type IF_1^{1-60}. Fig. 4E shows $k_{inhibition}^{app}$ of IF_1^{1-60}(Y33A), which follows a hyperbolic curve consistent with the two-step model of IF_1 inhibition. The plateau determined the k_{lock} of IF_1^{1-60}(Y33A) to be 0.019 s^{-1}, which is very similar to that of wild-type

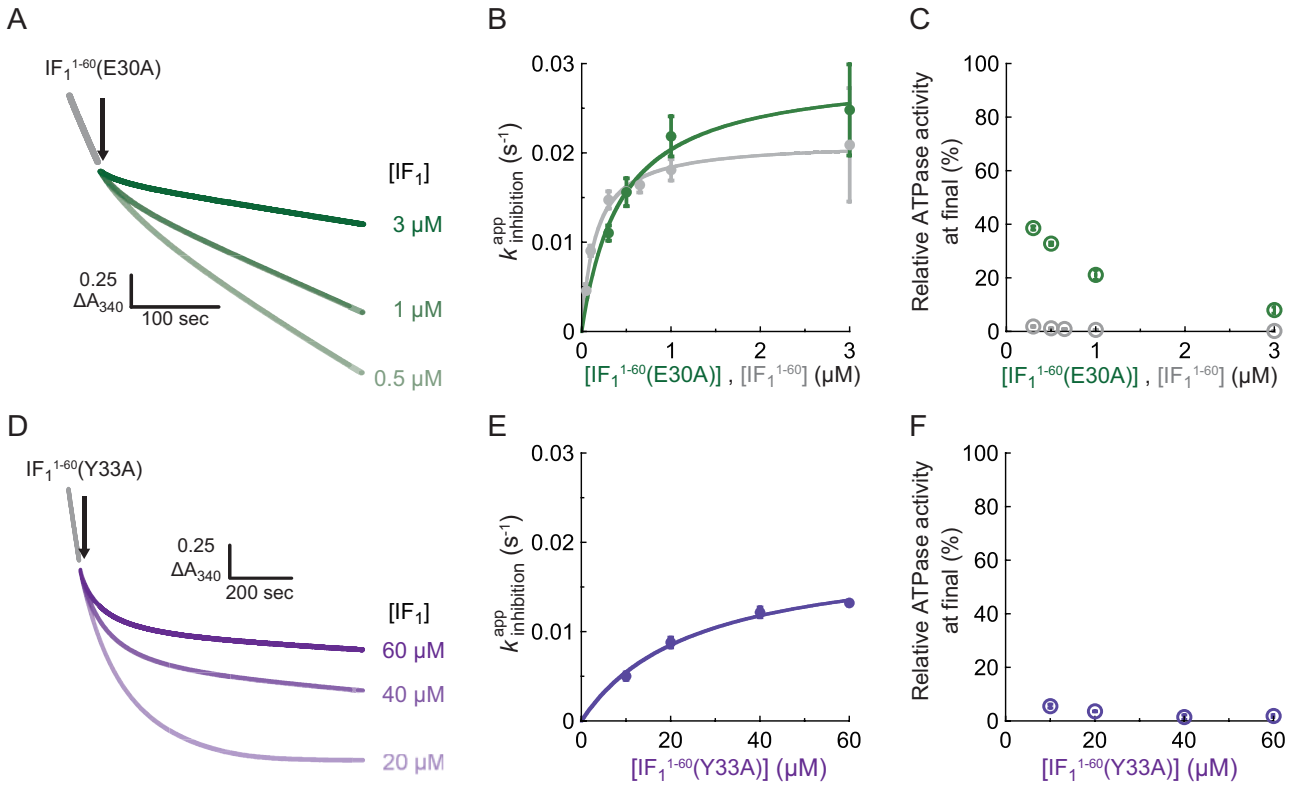

Fig. 4. Analysis of (*A–C*) IF_1^{1-60}(E30A) and (*D–F*) IF_1^{1-60}(Y33A) at 1 mM ATP. (**A**), (**D**) Time course of IF_1 inhibition for (A) IF_1^{1-60}(E30A) and (D) IF_1^{1-60}(Y33A). The final concentration of bMF_1 was 10 nM. (**B**), (**E**) Determined $k_{inhibition}^{app}$ plotted against [IF_1^{1-60}]s. Solid line represents the fitting curve of Eq. 2. (**C**), (**F**) Relative ATPase activity at the end of the measurement. The mean value and SD for each data point are shown with circles and error bars, respectively ($n = 3$ for each measurement). To see this figure in colour, go online.

IF_1^{1-60}. The significant difference was observed for $K_M^{IF_1}$, which was 25 μM in case of IF_1^{1-60}(Y33A), 160 times higher than that of wild-type IF_1^{1-60} (Table S2).

Thus, the effect of the mutations contradicted each other. Although the E30A mutant had normal $k_{inhibition}^{app}$, it was evidently deficient in locking the catalysis of F_1. The Y33A mutant was quite slow for the association with F_1 and had lower $k_{inhibition}^{app}$ and higher $K_M^{IF_1}$, although this mutant finally locked the catalysis almost completely.

Discussion

[ATP] dependence of k_{on}^{eff}

The present study showed that the effective binding rate of IF_1 to bMF_1, k_{on}^{eff}, evidently followed an [ATP]-dependent saturation curve (Fig. 3C). As IF_1 itself cannot bind ATP, the [ATP] dependence of k_{on}^{eff} can be attributed to bMF_1. As IF_1 inhibition requires catalytic turnover of bMF_1, it is reasonable to assume that the [ATP] dependence is the result of the Michaelis–Menten kinetics of ATPase activity. Kinetic analysis of bMF_1 rotation (*14*) shows that F_1 principally has two conformational states: binding dwell and catalytic dwell. Here, we neglect the short dwell between the binding dwell and the catalytic dwell because its duration is significantly shorter than those of the other dwells. The duration of the binding dwell is inversely proportional to [ATP] $\left(=1/(k_{on}^{ATP}[ATP])\right.$, whereas that of the catalytic dwell is constant at approximately 0.3 ms, irrespective of [ATP] (*14*). Thus, we consider the following two states of F_1:

$$F_1(\text{binding dwell}) \underset{k_{cat}^{ATP}}{\overset{k_{on}^{ATP}[ATP]}{\rightleftarrows}} F_1(\text{catalytic dwell})$$

where, k_{cat}^{ATP} represents the rate of the catalytic dwell ($\sim 2100\ s^{-1}$) and $k_{on}^{ATP}[ATP]$ is the rate of ATP binding to bMF_1. The simplest assumption to explain the [ATP] dependence of k_{on}^{eff} is that IF_1 preferentially associates with F_1 in the catalytic dwell. Here, we calculate the duty ratio of the catalytic dwell in the overall reaction time (R_c) as follows:

$$R_c = \frac{[ATP]}{K_m^{ATP} + [ATP]} \tag{5}$$

where, K_m^{ATP} is defined as $k_{cat}^{ATP}/k_{on}^{ATP}$ from the Michaelis–Menten fitting of the rotation speed, 77 μM (*14*). Along with Eq. (4) and Eq. (5), we redefine k_{on} and k_{on}^{eff} as follows:

$$k_{on} = R_c \cdot k_{on}' \tag{6}$$

$$k_{on}^{eff} = \frac{k_{lock}}{k_{off} + k_{lock}} \cdot k_{on} = \frac{k_{lock}}{k_{off} + k_{lock}} \cdot R_c \cdot k_{on}' \tag{7}$$

where, k_{on}' is the genuine rate constant of IF_1 binding to F_1 in the catalytic dwell. In Fig. 3C, the calculated R_c (orange) is plotted with the experimental data

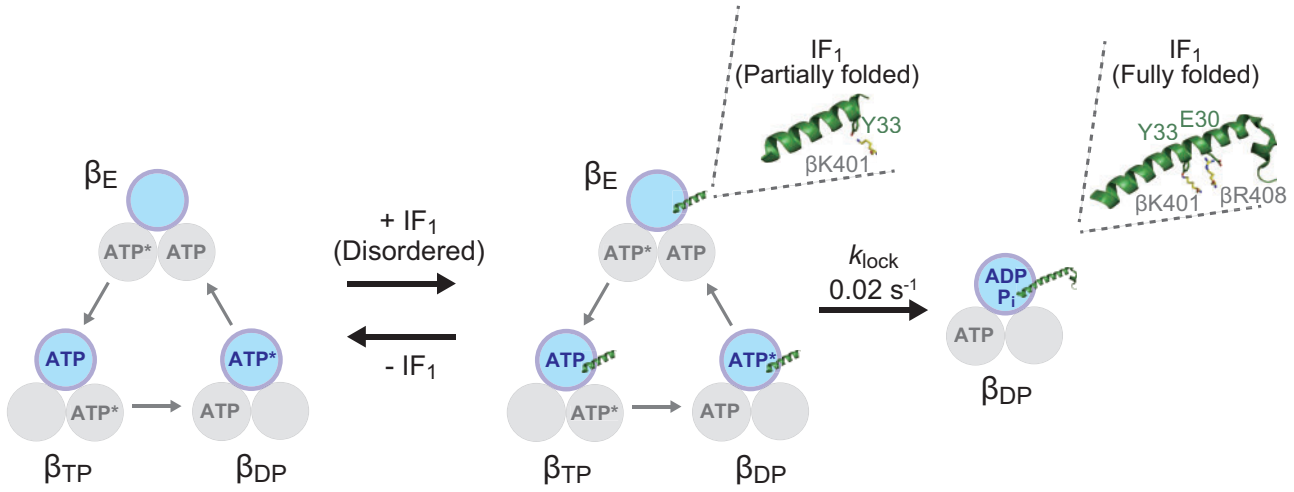

Fig. 5. The possible IF_1 inhibition scheme. Each circle represents the catalytic state of the β subunit. The asterisks following "ATP" represent the catalytically active state to undergo hydrolysis of a bound ATP. All nucleotide binding states of bMF_1 in this figure represent catalytic dwell, where bMF_1 executes cleavage of ATP. To see this figure in colour, go online.

points of k_{on}^{eff} (gray) after normalization. The experimental data points were fitted to determine $k_{on}^{'}$ and K_m^{ATP}. Since we have not estimated k_{off} from our experimental data, we simply assume k_{off} as $0.0017\,s^{-1}$, which was previously estimated (*30*). The resultant $k_{on}^{'}$ was determined to be $1.5 \times 10^5\ M^{-1}s^{-1}$, in good agreement with previous studies that determined $k_{on}^{'}$ in the order of 10^4–$10^6\ M^{-1}s^{-1}$ (*30*, *32*, *33*, *35*). However, K_m^{ATP} was determined to be 9 μM, which was obviously lower than the expected concentration of 77 μM. One of the possible explanations for this is the difference in experimental conditions: the rotation assay that determined K_m to be 77 μM selectively analysed actively rotating particles, whereas this study was based on a solution experiment where the value was averaged over molecules including those in the ADP-inhibited form. However, since the determined K_m from ATPase measurement was 218 μM (*14*), we do not have convincing interpretations at this moment. Future single-molecule analysis of IF_1 inhibition is required to overcome this limitation.

Proposed *IF_1* inhibition scheme and correlation with crystal structures

The present study observed hyperbolic curves at different [ATP]s that allows us to discuss the IF_1 inhibition mechanism based on the rotary catalysis of bMF_1. We also carefully examined the mutant IF_1s with a mutation at critical points: Glu30 and Tyr33. These mutants significantly affect the IF_1 inhibition at different processes. Taking the present results into account, together with those of previous single-molecule analyses (*14*) and structural studies (*31*), we propose the following IF_1-mediated inhibition mechanism (Fig. 5), where the role of Glu30 and Tyr33 in the two-step inhibition by IF_1 was clarified as well as the catalytic state of bMF_1. Initially, IF_1 weakly associates with F_1 in the catalytic dwell. This weakly bound state corresponds to the intermediate state in the two-step model, as represented $F_1 \cdot IF_1$ in Scheme 1, which undergoes reversible association and dissociation. We assume that this state represents IF_1 bound to the $\alpha_E\beta_E$ site in the crystal structure of the bMF_1-$(IF_1^{1-60})_3$ complex (*31*), where only a small part of the *N*-terminal helix is folded and associates with β_E via a few interactions at distal points to the γ subunit. In this state, a large part of the *N*-terminal helix remains unfolded and IF_1 principally does not interfere with γ rotation and catalysis. Tyr33 of IF_1 interacts with Lys401 of β_E in its crystal structure. The present study showed that Y33A mutation of IF_1 slows the association step of IF_1, in consistent with the crystal structure. Therefore, it is reasonable that the Y33A mutation largely suppresses the formation of the initial F_1-IF_1 complex.

After the formation of the initial F_1-IF_1 complex, IF_1 slowly transforms its conformation to the fully folded state, inserting the *N*-terminal helix deeply into the αβ interface, as seen in IF_1 at the $\alpha_{DP}\beta_{DP}$ site in its crystal structure. This state completely locks the rotation and catalysis of F_1 ($F_1 \cdot IF_1^{lock}$ in Scheme 1). In the crystal structure, Glu30 of IF_1 forms a salt bridge with Arg408 of β_{DP} or β_{TP} but not with Arg408 of β_E, indicating that Glu30 is involved in the isomerization of IF_1 to the fully stretched state. Consistent with this, the present study shows that the Ala mutant of Glu30 significantly destabilizes the locked state, without affecting formation of the initial F_1-IF_1 complex.

Notably, the mean duration for this isomerization from the initial F_1-IF_1 complex to the final locked state is 50 s ($= 1/k_{lock}$), which is significantly longer than the meantime for rotation (5–1000 ms). This suggests that F_1 drives thousands of γ rotation with a hanging IF_1. In other words, IF_1 almost always fails to isomerize to the locking state in each catalysis or each turn.

However, this contradicts the observation that IF_1 preferentially associates with F_1 in the catalytic dwell to form an initial complex. The contention that F_1 can drive many turns while associated with IF_1 indicates that F_1 has some affinity to IF_1 in any state

besides the catalytic dwell. Although we do not have clear explanations for this contradiction, simplification of the reaction scheme may be a possible cause. Nevertheless, the crystal structure suggests that IF_1 can have several conformations, and our model assumes only two states, neglecting intermediate states. Another possible reason for the contradiction is that some minor states were neglected through ensemble averaging and curve fitting of the time courses of IF_1 inhibition. Considering the intrinsic heterogeneity of the F_1 states among molecules, different experimental approaches that can assess molecular heterogeneity are required to resolve this problem and to elucidate the molecular mechanism of IF_1-mediated inhibition.

Supplementary Data

Supplementary Data are available at *JB* Online.

Acknowledgements

We thank M. Hara (University of Tokyo) for technical support, Chun-Biu Li (Stockholm University) for data analysis, and all members of the Noji laboratory for their valuable comments.

Funding

This work was supported in part by Grant-in-Aid for Scientific Research on Innovation Areas (JP18H04817, JP19H05380) from the Japan Society for the Promotion of Science (to H.U.).

Conflict of interest

None declared.

References

1. Walker, J.E.E. (2013) The ATP synthase: the understood, the uncertain and the unknown. *Biochem. Soc. Trans.* **41**, 1–16
2. Junge, W., Sielaff, H., and Engelbrecht, S. (2009) Torque generation and elastic power transmission in the rotary F_oF_1-ATPase. *Nature* **459**, 364–370
3. Mukherjee, S., Bora, R.P., and Warshel, A. (2015) Torque, chemistry and efficiency in molecular motors: a study of the rotary-chemical coupling in F_1-ATPase. *Q. Rev. Biophys.* **48**, 395–403
4. Weber, J. (2010) Structural biology: toward the ATP synthase mechanism. *Nat. Chem. Biol.* **6**, 794–795
5. Noji, H., Ueno, H., and McMillan, D.G.G. (2017) Catalytic robustness and torque generation of the F_1-ATPase. *Biophys. Rev.* **9**, 103–118
6. Noji, H., Ueno, H., and Kobayashi, R. (2020) Correlation between the numbers of rotation steps in the ATPase and proton-conducting domains of F- and V-ATPases. *Biophys. Rev.* **12**, 303–307
7. Spetzler, D., York, J., Daniel, D., Fromme, R., Lowry, D., and Frasch, W. (2006) Microsecond time scale rotation measurements of single F_1-ATPase molecules. *Biochemistry* **45**, 3117–3124
8. Abrahams, J.P., Leslie, A.G.W., Lutter, R., and Walker, J.E. (1994) Structure at 2.8 Å resolution of F1-ATPase from bovine heart mitochondria. *Nature* **370**, 621–628
9. Kabaleeswaran, V., Puri, N., Walker, J.E., Leslie, A.G.W., and Mueller, D.M. (2006) Novel features of the rotary catalytic mechanism revealed in the structure of yeast F_1 ATPase. *Embo J.* **25**, 5433–5442
10. Bowler, M.W., Montgomery, M.G., Leslie, A.G.W., and Walker, J.E. (2007) Ground state structure of F_1-ATPase from bovine heart mitochondria at 1.9 Å resolution. *J. Biol. Chem.* **282**, 14238–14242
11. Bason, J.V., Montgomery, M.G., Leslie, A.G.W., and Walker, J.E. (2015) How release of phosphate from mammalian F_1-ATPase generates a rotary substep. *Proc. Natl. Acad. Sci. USA* **112**, 6009–6014
12. Menz, R.I., Walker, J.E., and Leslie, A.G.W. (2001) Structure of bovine mitochondrial F_1-ATPase with nucleotide bound to all three catalytic sites: implications for the mechanism of rotary catalysis. *Cell* **106**, 331–341
13. Okazaki, K.-i., and Hummer, G. (2013) Phosphate release coupled to rotary motion of F_1-ATPase. *Proc. Natl. Acad. Sci. USA* **110**, 16468–16473
14. Kobayashi, R., Ueno, H., Li, C.-B.B., and Noji, H. (2020) Rotary catalysis of bovine mitochondrial F_1 -ATPase studied by single-molecule experiments. *Proc. Natl. Acad. Sci. USA.* **117**, 1447–1456
15. Okuno, D., Fujisawa, R., Iino, R., Hirono-Hara, Y., Imamura, H., and Noji, H. (2008) Correlation between the conformational states of F_1-ATPase as determined from its crystal structure and single-molecule rotation. *Proc. Natl. Acad. Sci. USA* **105**, 20722–20727
16. Shimabukuro, K., Yasuda, R., Muneyuki, E., Hara, K.Y., Kinosita, K., and Yoshida, M. (2003) Catalysis and rotation of F_1 motor: cleavage of ATP at the catalytic site occurs in 1 ms before 40° substep rotation. *Proc. Natl. Acad. Sci. USA* **100**, 14731–14736
17. Feniouk, B.A., Suzuki, T., and Yoshida, M. (2006) The role of subunit epsilon in the catalysis and regulation of F_OF_1-ATP synthase. *Biochim. Biophys. Acta* **1757**, 326–338
18. Mendoza-Hoffmann, F., Zarco-Zavala, M., Ortega, R., and García-Trejo, J.J. (2018) Control of rotation of the F_1F_O-ATP synthase nanomotor by an inhibitory α-helix from unfolded ε or intrinsically disordered ζ and IF_1 proteins. *J. Bioenerg. Biomembr.* **50**, 403–424
19. Krah, A. (2015) Linking structural features from mitochondrial and bacterial F-type ATP synthases to their distinct mechanisms of ATPase inhibition. *Prog. Biophys. Mol. Biol.* **119**, 94–102
20. Hirono-Hara, Y., Noji, H., Nishiura, M., Muneyuki, E., Hara, K.Y., Yasuda, R., Kinosita, K., and Yoshida, M. (2001) Pause and rotation of F_1-ATPase during catalysis. *Proc. Natl. Acad. Sci. USA* **98**, 13649–13654
21. McMillan, D.G.G., Watanabe, R., Cook, G.M., Ueno, H., and Noji, H. (2016) Biophysical characterization of a thermoalkaliphilic molecular motor with a high stepping torque gives insight into evolutionary ATP synthase adaptation. *J. Biol. Chem.* **291**, 23965–23977
22. Runswick, M.J., Bason, J.V., Montgomery, M.G., Robinson, G.C., Fearnley, I.M., and Walker, J.E. (2013) The affinity purification and characterization of ATP synthase complexes from mitochondria. *Open Biol.* **3**, 120160.
23. Pullman, M.E., and Monroy, G.C. (1963) A naturally occurring inhibitor of mitochondrial adenosine triphosphatase. *J.Biol. Chem.* **238**, 3762–3769
24. Sánchez-Cenizo, L., Formentini, L., Aldea, M., Ortega, Á.D., García-Huerta, P., Sánchez-Aragó, M., and Cuezva, J.M. (2010) Up-regulation of the ATPase Inhibitory Factor 1 (IF_1) of the mitochondrial H^+-ATP

synthase in human tumors mediates the metabolic shift of cancer cells to a warburg phenotype. *J. Biol. Chem.* **285**, 25308–25313
25. Gómez-Puyou, A., de Gómez-Puyou, M.T., and Ernster, L. (1979) Inactive to active transitions of the mitochondrial ATPase complex as controlled by the ATPase inhibitor. *Biochim. Biophys. Acta - Bioenerg.* **547**, 252–257
26. Gordon-Smith, D.J., Carbajo, R.J., Yang, J.C., Videler, H., Runswick, M.J., Walker, J.E., and Neuhaus, D. (2001) Solution structure of a C-terminal coiled-coil domain from Bovine IF_1: the inhibitor protein of F_1 ATPase. *J. Mol. Biol.* **308**, 325–339
27. Cabezón, E., Arechaga, I., Jonathan, P., Butler, G., and Walker, J.E. (2000) Dimerization of bovine F_1-ATPase by binding the inhibitor protein, IF_1. *J. Biol. Chem.* **275**, 28353–28355
28. Gledhill, J.R., Montgomery, M.G., Leslie, A.G.W., and Walker, J.E. (2007) How the regulatory protein, IF_1, inhibits F1-ATPase from bovine mitochondria. *Proc. Natl. Acad. Sci. USA***104**, 15671–15676
29. Van Raaij, M.J., Orriss, G.L., Montgomery, M.G., Runswick, M.J., Fearnley, I.M., Skehel, J.M., and Walker, J.E. (1996) The ATPase inhibitor protein from bovine heart mitochondria: the minimal inhibitory sequence. *Biochemistry* **35**, 15618–15625
30. Bason, J.V., Runswick, M.J., Fearnley, I.M., and Walker, J.E. (2011) Binding of the inhibitor protein IF_1 to bovine F_1-ATPase. *J. Mol. Biol.* **406**, 443–453
31. Bason, J.V., Montgomery, M.G., Leslie, A.G.W., and Walker, J.E. (2014) Pathway of binding of the intrinsically disordered mitochondrial inhibitor protein to F_1-ATPase. *Proc. Natl. Acad. Sci. USA* **111**, 11305–11310
32. Corvest, V., Sigalat, C., Venard, R., Falson, P., Mueller, D.M., and Haraux, F. (2005) The binding mechanism of the yeast F_1-ATPase inhibitory peptide: role of catalytic intermediates and enzyme turnover. *J. Biol. Chem.* **280**, 9927–9936
33. Corvest, V., Sigalat, C., and Haraux, F. (2007) Insight into the bind-lock mechanism of the yeast mitochondrial ATP synthase inhibitory peptide. *Biochemistry* **46**, 8680–8688
34. Klein, G., Satre, M., and Vignais, P. (1977) Natural protein ATPase inhibitor from *Candida utilis* mitochondria binding properties of the radiolabeled inhibitor. *FEBS Lett.* **84**, 129–134
35. Milgrom, Y.M. (1989) An ATP dependence of mitochondrial F_1-ATPase inactivation by the natural inhibitor protein agrees with the alternating-site binding-change mechanism. *FEBS Lett.* **246**, 202–206
36. Wu, Q., Andrianaivomananjaona, T., Tetaud, E., Corvest, V., and Haraux, F. (2014) Interactions involved in grasping and locking of the inhibitory peptide IF_1 by mitochondrial ATP synthase. *Biochim. Biophys. Acta* **1837**, 761–772
37. Cintrón, N.M., Hullihen, J., Schwerzmann, K., and Pedersen, P.L. (1982) Proton-adenosinetriphosphatase complex of rat liver mitochondria: effect of its inhibitory peptide on adenosine 5′-triphosphate hydrolytic and functional activities of the enzyme. *Biochemistry* **21**, 1878–1885
38. Gomez-Fernandez, J.C., and Harris, D.A. (1978) A thermodynamic analysis of the interaction between the mitochondrial coupling adenosine triphosphatase and its naturally occurring inhibitor protein. *Biochem. J.* **176**, 967–975
39. Chernyak, B.V., Khodjaev, E.Y., and Kozlov, I.A. (1985) The oxidation of sulfhydryl groups in mitochondrial F_1-ATPase decreases the rate of its inactivation by the natural protein inhibitor. *FEBS Lett.* **187**, 253–256
40. Panchenko, M.V., and Vinogradov, A.D. (1985) Interaction between the mitochondrial ATP synthetase and ATPase inhibitor protein. Active/inactive slow pH-dependent transitions of the inhibitor protein. *FEBS Lett.* **184**, 226–230
41. Hayashi, S., Ueno, H., Shaikh, A.R., Umemura, M., Kamiya, M., Ito, Y., Ikeguchi, M., Komoriya, Y., Iino, R., and Noji, H. (2012) Molecular mechanism of ATP hydrolysis in F_1-ATPase revealed by molecular simulations and single-molecule observations. *J. Am. Chem. Soc.* **134**, 8447–8454